Maximum Quantum Work at Criticality: Stirling Engines and Fibonacci-Lucas Degeneracies

Bastian Castorene •, 1, 2, * Martin HvE Groves •, 2 Francisco J. Peña •, 2 Eugenio E. Vogel •, 3, 4 and Patricio Vargas • 2

1 Instituto de Física, Pontificia Universidad Católica de Valparaíso, Casilla 4950, 2373223 Valparaíso, Chile
2 Departamento de Física, Universidad Técnica Federico Santa María, 2390123 Valparaíso, Chile
3 Departamento de Ciencias Físicas, Universidad de La Frontera, Casilla 54-D, Temuco 4811230, Chile
4 Facultad de Ingeniería y Arquitectura, Universidad Central de Chile, Av. Sta. Isabel 1186, Santiago 8330601, Chile
(Dated: October 31, 2025)

Many-body effects and quantum criticality play a central role in determining the performance of quantum thermal machines. Although operating near a quantum critical point (QCP) is known to enhance engine performance, the precise thermodynamic conditions required to attain the Carnot efficiency limit remain unsettled. Here, we derive the exact conditions for a quantum Stirling engine to achieve Carnot efficiency when a QCP drives its working medium. In the low-temperature regime, where only the ground-state manifold is populated, the net work output is given by $W = k_B \delta \ln(g_{\rm crit}/g_0)$ with $\delta = T_H - T_L$, which directly yields the Carnot efficiency $\eta_C = 1 - T_L/T_H$, independent of microscopic details. Notably, whereas ideal Stirling cycles attain Carnot efficiency only with a perfect regenerator, here no regenerator is required because, at low temperatures, the thermal population remains confined to the degenerate ground state; this represents a clear quantum advantage over engines with classical working substances. We validate this universal result by recovering known behaviors in various quantum systems, including spin chains with Dzyaloshinskii-Moriya interactions and magnetic anisotropies. Applying the framework to the one-dimensional antiferromagnetic Ising model, we predict non-extensive scaling of the work output governed by Fibonacci and Lucas numbers for open chains and closed rings, respectively, which converges to classical extensivity in the thermodynamic limit. This analysis establishes a general and robust foundation for designing quantum thermal machines that reach the Carnot bound while delivering finite work.

I. INTRODUCTION

Quantum thermodynamics investigates how quantum principles govern energy exchange and conversion at microscopic scales [1–13]. A central objective is to develop and analyze quantum thermal machines such as engines, refrigerators, and heat pumps operating in the quantum regime that may exploit coherence, entanglement, many-body effects, flat bands, and others to surpass classical performance benchmarks [1, 14–17].

Among quantum cycles, the Stirling cycle has attracted sustained interest due to its conceptual simplicity and experimental accessibility to obtain finite work with highly efficiency [18–21]. It consists of two isothermal and two isoparametric (or isochoric) processes, providing a versatile setting to probe performance limits. A recurring observation is that tuning the working medium near a quantum critical point (QCP) can markedly enhance performance [22–27]. A QCP triggered at zero temperature by varying an external control parameter, such as field or pressure, features qualitative ground-state changes, divergent correlation lengths, and universal scaling [28]. The associated large density of states and enhanced fluctuations are widely regarded as a resource for thermodynamic tasks.

Extensive studies across diverse platforms, including Heisenberg spin chains [29–32], anisotropic qubit systems [33, 34], and models with Dzyaloshinskii–Moriya interactions [35–38], have reported enhanced work output and efficiency when thermodynamic cycles operate across a QCP. Nevertheless, a general and exact analytical characterization of the necessary and sufficient conditions to attain Carnot efficiency in critical quantum Stirling engines has remained open, with many results relying on numerics or model-specific features, leaving questions about universality and the role of ground-state degeneracies.

Here we present a general analytical framework for Stirling engines operating at a QCP. We show that, in the low-temperature and large-gap regime, a cycle executed between a critical point with degeneracy g_{crit} and a high-field point with degeneracy g_0 achieves precisely Carnot efficiency, with net work given by a simple universal expression that depends only on the reservoir temperatures and the degeneracy ratio. We validate this result by quantitative agreement with previously reported systems ranging from two-qubit setups to extended spin chains with nontrivial interactions. We further apply the framework to the one-dimensional antiferromagnetic Ising model [39–41], unveiling

^{*} bastian.castorene.c@mail.pucv.cl

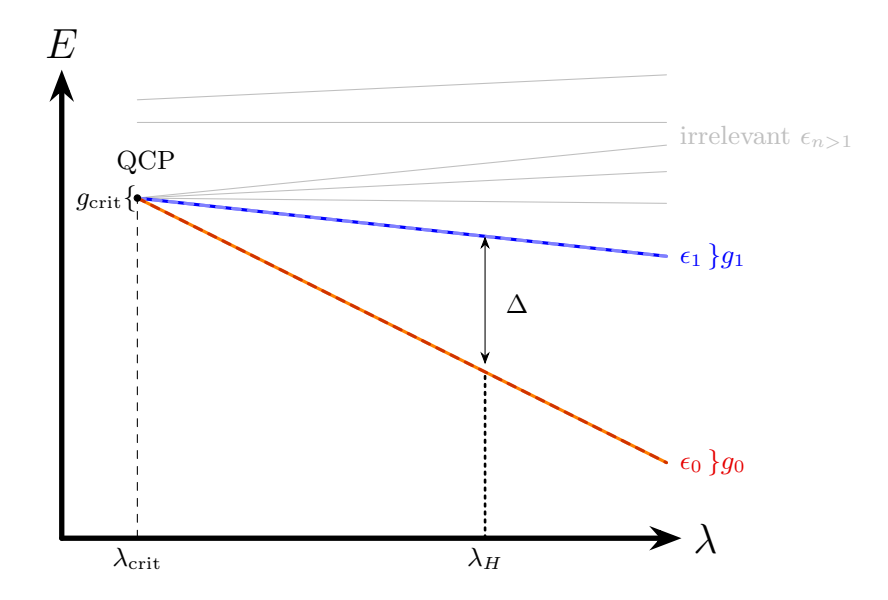


FIG. 1: Schematic diagram of energy E versus the tuning parameter λ . At the QCP located at $\lambda_{\rm crit}$, the $g_{\rm crit}$ -fold degenerate ground state energy levels separate. The new ground state ϵ_0 with degeneracy g_0 and the first excited state ϵ_1 with degeneracy g_1 are separated by an energy gap Δ at high tuning parameter values λ_H . The thermal populations of higher excited states (with energies $\epsilon_{n>1}$) are negligible near absolute zero; only their degeneracies at the QCP influence the thermodynamic properties of the system.

a connection to number theory: the work scales with the logarithm of Fibonacci numbers for open chains and Lucas numbers for rings, revealing a non-extensive quantum effect that disappears only in the macroscopic limit. Notably, this critical-cycle route to Carnot efficiency does not require a classical regenerator.

In summary, our framework consolidates diverse findings into a unified theory and establishes experimentally testable conditions for quantum thermal machines to attain the fundamental efficiency limit with finite work output.

II. MODEL

The working medium consists of any physical system whose energy spectrum can be tuned by an external parameter λ , and which exhibits a QCP at $\lambda = \lambda_{\rm crit}$ when the temperature approaches absolute zero. At the QCP, the system undergoes a fundamental transformation characterized by symmetry breaking and qualitative changes in the ground state structure.

As illustrated in Fig. 1, the g_{crit} -fold degenerate ground state at the QCP splits due to interactions with the tuning parameter. For $\lambda > \lambda_{\text{crit}}$, the lowest-energy states separates into a ground state ϵ_0 with degeneracy g_0 and an excited level ϵ_1 characterized by degeneracy g_1 . At sufficiently large values of the tuning parameter (λ_H) , these two levels are separated by an energy gap Δ .

Higher excited states $\epsilon_{n>1}$ play a negligible role in this regime. Near absolute zero temperature, the thermal population of these states becomes vanishingly small due to the Boltzmann suppression factor. Even at the QCP, the available thermal energy remains insufficient to significantly populate levels beyond the critic ground state. Only the degeneracies of these higher energy levels at $\lambda_{\rm crit}$ can influence the thermodynamic properties of the system through their contribution to the density of states at the critical point.

The thermodynamic properties of the system can be calculated and fully characterized through the canonical partition function. Taking into account that at absolute zero each energy level E_i may be g_i -fold degenerate, the partition function is given by:

$$Z_{\lambda}(T) = \sum_{i} g_{i} \exp\left(-\frac{E_{i}(\lambda)}{k_{B}T}\right) \tag{1}$$

The thermal equilibrium populations follow directly from the partition function through the Boltzmann distribution:

$$p_i(\lambda) \equiv \frac{g_i e^{-\beta E_i(\lambda)}}{Z_\lambda}, \text{ where } \beta = \frac{1}{k_B T}.$$
 (2)

From the partition function and the associated Boltzmann probabilities, the standard relations of canonical ensemble thermodynamics yield the Helmholtz free energy, entropy, and internal energy:

$$F_{\lambda}(T) = -k_B T \ln Z_{\lambda}(T),\tag{3}$$

$$S_{\lambda}(T) = -k_B \sum_{i} p_i \ln p_i = -\left(\frac{\partial F_{\lambda}(T)}{\partial T}\right) \Big|_{\lambda}, \tag{4}$$

$$U_{\lambda}(T) = \sum_{i} p_{i} E_{i} = k_{B} T^{2} \left(\frac{\partial \ln Z_{\lambda}(T)}{\partial T} \right) \bigg|_{\lambda}.$$
 (5)

It is crucial to emphasize that in the zero-temperature limit for the two tuning parameters λ_{crit} and λ_H shown in Fig. 1, the internal energy reduces to the ground state energy, while the entropy, in analogy to the microcanonical ensemble formulation, is determined by counting the number of states sharing the same minimum energy, that is, the degeneracy of the ground state at each parameter value:

$$U_{\lambda_{\text{crit}}}(T \to 0) = \epsilon_{\text{ground}}^{(\text{crit})} \implies S_{\lambda_{\text{crit}}}(T \to 0) = k_B \ln(g_{\text{crit}})$$

$$U_{\lambda_H}(T \to 0) = \epsilon_0 \implies S_{\lambda_H}(T \to 0) = k_B \ln(g_0)$$
(6)

III. STIRLING CYCLE AND CRITICALLITY

A. General Theory of the Quantum Stirling Cycle

The Stirling cycle is characterized by four stages: two isothermal processes and two isoparametric processes (where the tuning parameter λ is held constant). Unlike the well-known Otto cycle, the net heat and work contributions in each segment are not directly evident from the trajectory of the cycle alone. Instead, they must be determined by analyzing the entropy differences at each stage point throughout the complete cycle.

The isoparametric stages are analogous to the isochoric processes in a classical ideal-gas Stirling cycle, where volume is fixed. In quantum and condensed matter systems, the fixed parameter λ may represent various external controls such as magnetic field, electric field, exchange interactions, or mechanical stress, among others. During the isothermal processes, the system remains in thermal equilibrium with the hot and cold reservoirs at temperatures T_H and T_L ($T_H > T_L$), while the tuning parameter varies between λ_L and λ_H ($\lambda_H > \lambda_L$).

During the isoparametric stages, the system undergoes temperature exchange at fixed parameter value. Consequently, no work is performed since the tuning parameter remains constant. The cycle representation in Fig. 2 will be analyzed stage-by-stage. It should be noted that any other intrinsic parameters of the system remain fixed throughout the cycle $A \to B \to C \to D \to A$; only the temperature T and tuning parameter λ are varied.

 $A \to B$.: Isothermal compression at $T = T_H$. The tuning parameter varies from λ_H to λ_L while the system maintains thermal equilibrium with the hot reservoir. The heat exchange during this process is given by the entropy change:

$$Q_{AB} = T_H [S_{\lambda_L}(T_H) - S_{\lambda_H}(T_H)] \tag{7}$$

 $\mathbf{B} \to \mathbf{C}$: Isoparametric cooling at constant $\lambda = \lambda_L$. Decoupling from the hot reservoir and cooling to T_L decreases the internal energy without work performance:

$$Q_{BC} = U_{\lambda_L}(T_L) - U_{\lambda_L}(T_H) \tag{8}$$

 $\mathbf{C} \to \mathbf{D}$: Isothermal expansion at $T = T_L$. The tuning parameter returns from λ_L to λ_H while the system equilibrates with the cold reservoir. The associated heat transfer is:

$$Q_{CD} = T_L[S_{\lambda_H}(T_L) - S_{\lambda_L}(T_L)] \tag{9}$$

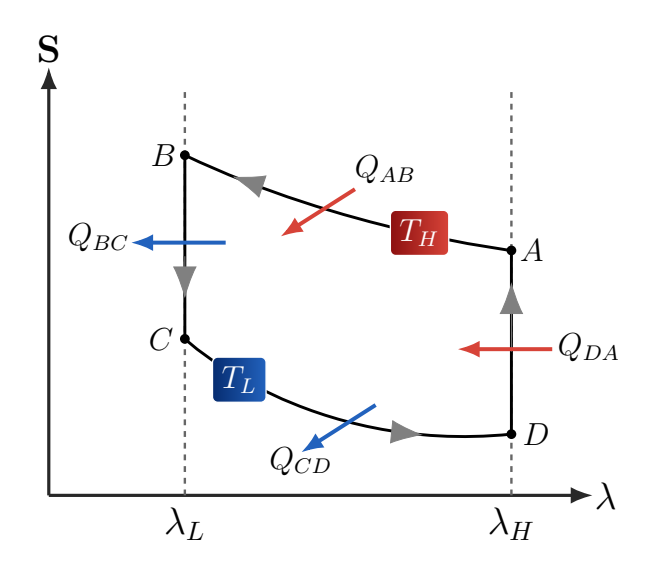


FIG. 2: Schematic representation of the Stirling cycle in terms of entropy and the control parameter λ . Segments AB and CD correspond to the isothermal processes at $T = T_H$ and $T = T_L$, respectively. The entropy at point A(D) is lower than at point B(C), and the cycle proceeds in a counterclockwise direction.

 $\mathbf{D} \to \mathbf{A}$: Isoparametric heating at constant $\lambda = \lambda_H$. Heating from T_L to T_H increases the internal energy, again without work being performed:

$$Q_{DA} = U_{\lambda_H}(T_H) - U_{\lambda_H}(T_L) \tag{10}$$

From the first law of thermodynamics, the internal energy variation over a closed cycle is zero:

$$dU = dQ + dW = \sum_{i} E_{i} dp_{i} + \sum_{i} p_{i} dE_{i}, \quad \Longrightarrow \quad \oint dU = 0.$$
(11)

For this cycle, the total net work equals the sum of heat exchanges during each stage:

$$W = Q_{AB} + Q_{BC} + Q_{CD} + Q_{DA} = Q_H + Q_L. (12)$$

We adopt the sign convention where positive (negative) heat Q indicates that the system absorbs (releases) heat. For the cycle shown in Fig. 2, the net heat exchanges are $Q_H = Q_{AB} + Q_{DA} > 0$ (absorbed from hot reservoir) and $Q_L = Q_{CD} + Q_{BC} < 0$ (released to cold reservoir). Similarly, positive (negative) work W indicates work done by (on) the system.

In the context of a heat engine performing useful work, the Stirling engine efficiency η is defined as the ratio between the total net work and the heat absorbed from the hot reservoir:

$$\eta = \frac{Q_H + Q_L}{Q_H} = \frac{W}{Q_H} = 1 - \left| \frac{Q_{CD} + Q_{BC}}{Q_{AB} + Q_{DA}} \right|. \tag{13}$$

Depending on the system's fundamental properties, the signs of work and heat may differ from those of a conventional heat engine. By reversing the cycle direction, a refrigerator can be obtained where previously there was an engine. Similarly, by applying substantial work to the system, it can extract heat from the cold reservoir and function as a heat pump. Furthermore, within the formalism of quantum thermodynamics, two additional exotic regimes exist: the accelerator and the heater. All these operational modes are summarized in the heat-work sign table in Table I.

B. Quantum Stirling Engines at Quantum Criticality

While the general Stirling cycle shown in Fig. 2 works effectively for a system at quantum criticality as in Fig. 1, a specific diagram is necessary to illustrate the exact behavior. As illustrated in Fig. 3, the thermodynamic cycle is performed by sweeping the control parameter from the QCP λ_{crit} (Fig. 1) to a high parameter value λ_H , with

TABLE I: Signs	of heat and	total work	used to clas	ssify different	operational	regimes

Operational regime	W	$Q_{\rm in}$	Q_{out}
Engine	> 0	> 0	< 0
Refrigerator	< 0	< 0	> 0
Heat pump	< 0	> 0	> 0
Heater	< 0	< 0	< 0
Accelerator	< 0	> 0	< 0

 $\lambda_L = \lambda_{\rm crit}$. Alternatively, by choosing to vary the high parameter λ_H while keeping λ_L fixed, the diagram becomes reflected horizontally, with point A corresponding to the ground state at the higher temperature. Similarly, if the high field is selected as the control parameter, the cycle can be defined by assigning either the initial or the final point to coincide with the QCP.

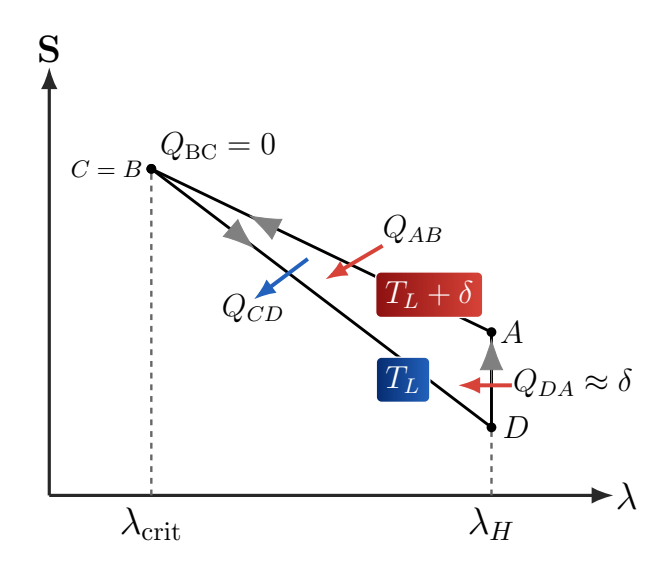


FIG. 3: Stirling cycle diagram for a system with a QCP, represented in terms of entropy and the control parameter λ . The critical value $\lambda_{\rm crit}$ denotes the QCP. Segments AB and CD correspond to the isothermal processes at $T_H = T_L + \delta$ and T_L , respectively. The entropy satisfies $S_B = S_C = g_{\rm crit}$, while $S_D = g_0$ and S_A may include contributions from g_1 . The heat exchange along BC vanishes $(Q_{BC} = 0)$, whereas Q_{DA} is proportional to the temperature difference between reservoirs.

The thermal reservoirs are considered to be close in temperature, with $(T_H - T_L)/T_H = \delta/T_H \ll 1$, so that T_H may be written as $T_H = T_L + \delta$ to leading order. This condition ensures that when the system is at the QCP, the entropy is dominated by the ground-state degeneracy, with negligible population of excited states. Consequently, the internal energy at the critical point becomes temperature-independent and constant for both reservoir temperatures, since they are both small and closely spaced.

Additionally, the low-temperature regime guarantees that at high tuning parameter λ_H , predominantly the ground state is populated, while the first excited state remains scarcely occupied and higher levels are empty. The energy gap Δ between the ground and first excited states determines the characteristic energy scale, and the internal energy at both low and high temperatures is governed by this parameter. Later in this section, the case of a reduced energy gap will be considered, where thermal occupation of the first excited state becomes non-negligible even at low temperatures.

For the present discussion, in the very low-temperature regime and under the assumption of a large energy gap Δ , the relevant thermodynamic quantities at each stage of the cycle are:

(A) **Point A** (λ_H, T_H) : The internal energy approaches the ground state energy ϵ_0 , and the entropy corresponds solely to the ground state degeneracy:

$$U_{\lambda_H}^{(A)}(T_H) \simeq \epsilon_0,$$
 $S_{\lambda_H}^{(A)}(T_H) = k_B \ln(g_0).$ (14)

(B) **Point B** (λ_{crit} , T_H): Despite the higher temperature, the internal energy remains at the critical ground state energy, and the entropy reflects the QCP degeneracy. The thermal energy is insufficient to significantly populate excited states:

$$U_{\lambda_{\text{crit}}}^{(B)}(T_H) = \epsilon_{\text{ground}}^{(\text{crit})}, \qquad S_{\lambda_{\text{crit}}}^{(B)}(T_H) = k_B \ln(g_{\text{crit}}).$$
 (15)

(C) Point C (λ_{crit}, T_L): The internal energy remains constant at the critical ground state value, and the entropy again reflects the QCP degeneracy:

$$U_{\text{crit}}^{(B)}(T_H)U_{\lambda_{\text{crit}}}^{(C)}(T_L) = \epsilon_{\text{ground}}^{(\text{crit})}, \qquad S_{\lambda_{\text{crit}}}^{(C)}(T_L) = k_B \ln(g_{\text{crit}}).$$
 (16)

(D) **Point D** (λ_H, T_L) : The entropy is determined by the ground state degeneracy at λ_H , and the internal energy approaches ϵ_0 , as the temperature cannot populate excited states:

$$U_{\lambda_H}^{(D)}(T_L) \simeq \epsilon_0, \qquad S_{\lambda_H}^{(D)}(T_L) = k_B \ln(g_0). \tag{17}$$

Thus, using the thermodynamic functions presented in Eqs. (14-17), the heat exchanges for each stage of the Stirling cycle are explicitly analyzed:

$$Q_{AB} = T_H \left[S_{\lambda_{\text{crit}}}^{(B)}(T_H) - S_{\lambda_H}^{(A)}(T_H) \right] = k_B T_H [\ln(g_{\text{crit}}) - \ln(g_0)] = k_B T_H \ln\left(\frac{g_{\text{crit}}}{g_0}\right), \tag{18}$$

$$Q_{BC} = U_{\lambda_{\text{crit}}}^{(C)}(T_L) - U_{\lambda_{\text{crit}}}^{(B)}(T_H) = 0, \tag{19}$$

$$Q_{CD} = T_L \left[S_{\lambda_H}^{(D)}(T_L) - S_{\lambda_{\text{crit}}}^{(C)}(T_L) \right] = k_B T_L [\ln(g_0) - \ln(g_{\text{crit}})] = -k_B T_L \ln\left(\frac{g_{\text{crit}}}{g_0}\right), \tag{20}$$

$$Q_{DA} = U_{\lambda_H}^{(A)}(T_H) - U_{\lambda_H}^{(D)}(T_L) = 0.$$
(21)

Thus, the work performed in the Stirling cycle can be expressed as the sum of the exchanged heats. Assuming that the hot reservoir is set as $T_H = T_L + \delta$, the net work becomes

$$W = k_B (T_H - T_L) \ln \left(\frac{g_{\text{crit}}}{g_0}\right), \tag{22}$$

$$W = k_B \delta \ln \left(\frac{g_{\text{crit}}}{g_0}\right). \tag{23}$$

$$W = k_B \delta \ln \left(\frac{g_{\text{crit}}}{g_0} \right). \tag{23}$$

where $g_{\rm crit}$ and g_0 denote the ground-state degeneracies at the critical and high-field points, respectively, and δ represents the temperature difference between the reservoirs. By construction, the engine efficiency is identical to the Carnot efficiency.

$$\eta_C = \frac{k_B T_H \ln\left(\frac{g_{\text{crit}}}{g_0}\right) - k_B T_L \ln\left(\frac{g_{\text{crit}}}{g_0}\right)}{k_B T_H \ln\left(\frac{g_{\text{crit}}}{g_0}\right)} = 1 - \frac{T_L}{T_H} = \frac{1}{1 + \frac{T_L}{\delta}}.$$
 (24)

Notably, while ideal Stirling cycles reach Carnot efficiency only in the presence of a perfect regenerator, in Eq. (24) no regenerator is required. At low temperatures, the thermal population remains confined within the degenerate ground-state manifold, representing a distinct quantum advantage over engines operating with classical working substances.

If the machine operates as a refrigerator, either by reversing the cycle direction or due to intrinsic system properties, the coefficient of performance (COP_R) can be defined as an analog to the engine efficiency. However, unlike the efficiency, the COP has no upper bound. For this analysis, the cycle in Fig. 3 is reversed, consequently inverting the labels identifying the stages. The resulting coefficient satisfies the Carnot refrigerator condition:

$$COP_R = \frac{Q_{\text{out}}}{|W|} = \frac{Q_{DC} + Q_{CB}}{|Q_{AD} + Q_{DC} + Q_{CB} + Q_{BA}|},$$
 (25)

$$COP_{R} = \frac{k_{B}T_{L}\ln\left(\frac{g_{\text{crit}}}{g_{0}}\right)}{k_{B}T_{H}\ln\left(\frac{g_{\text{crit}}}{g_{0}}\right) - k_{B}T_{L}\ln\left(\frac{g_{\text{crit}}}{g_{0}}\right)},\tag{26}$$

$$COP_R^{(C)} = \frac{T_L}{T_H - T_L} = \frac{T_L}{\delta}.$$
 (27)

Similarly, if the machine operates as a heat pump, the coefficient of performance (COP_{HP}) is defined as the ratio between the heat delivered to the hot reservoir and the net work performed on the system. In our cycle, the heat absorbed by the hot reservoir corresponds to Q_{AB} , while the net work is the sum of all heat exchanges. Thus, the (COP_{HP}) can be expressed as:

$$COP_{HP} = \frac{Q_{in}}{|W|} = \frac{Q_{BA} + Q_{AD}}{Q_{DA} + Q_{DC} + Q_{CB} + Q_{BA}},$$
(28)

$$COP_{HP} = \frac{k_B T_H \ln\left(\frac{g_{crit}}{g_0}\right)}{k_B (T_H - T_L) \ln\left(\frac{g_{crit}}{g_0}\right)},$$
(29)

$$COP_{HP}^{(C)} = COP_{R}^{(C)} + 1 = \frac{T_H}{T_H - T_L} = \frac{T_H}{\delta}.$$
 (30)

In the following subsection, the effect of a small energy gap is analyzed, where the first excited state can be thermally occupied even for a small temperature increment δ .

C. Thermal Excitations and Small-Gap Effects

To evaluate the effect of higher energy-level occupation on the system's work and heat exchange, we consider that partial population of the first excited state occurs only when the system is in contact with the hot reservoir at temperature $T_H = T_L + \delta$ and high fixed parameter λ_H , corresponding to point A in Fig. 3. This contribution is treated as a small perturbation, since the other thermodynamic points remain unaffected. The low temperature T_L ensures that only the ground state is populated at point D.

Accordingly, the correction is localized at point A and can be described using an effective two-level model within the canonical ensemble, where the energy gap Δ in Fig. 1 is sufficiently small to allow partial excitation of the first excited state:

$$Z_{\lambda_H}(T) = g_0 e^{-\frac{\epsilon_0}{k_B T}} + g_1 e^{-\frac{\epsilon_0 + \Delta}{k_B T}}, \qquad \Delta = \epsilon_1 - \epsilon_0.$$
(31)

Where g_i are the degeneracies of the ground-state ϵ_0 and the first excited state ϵ_1 , respectively. Using the standard relations of the canonical ensemble and defining Δ as the energy gap between the first excited state and the groundstate, the Helmholtz free energy of the system becomes:

$$F_{\lambda_H}(T) = -k_B T \ln\left(Z_{\lambda_H}(T)\right) = -k_B T \ln\left(e^{-\frac{\epsilon_0}{k_B T}} \left[g_0 + g_1 e^{-\frac{\Delta}{k_B T}}\right]\right),\tag{32}$$

$$F_{\lambda_H}(T) = \epsilon_0 - k_B T \ln g_0 - k_B T \ln \left(1 + \frac{g_1}{g_0} e^{-\frac{\Delta}{k_B T}} \right). \tag{33}$$

From the free energy, the internal energy can be calculated, and the entropy can be expressed using the corresponding Legendre transformation for the internal energy as

$$U_{\lambda_H}(T) = k_B T^2 \frac{\partial \ln Z_{\lambda_H}}{\partial T} \bigg|_{\lambda_H}, \qquad TS_{\lambda_H}(T) = U_{\lambda_H}(T) - F_{\lambda_H}(T). \tag{34}$$

Expressing the entropy in Eq. (34) in terms of the internal and Helmholtz free energies is convenient, as only the latter contributes across the cycle. Consequently, the perturbation affects solely the heat exchange at point A. The

heat Q_{AB} of the first isothermal process can thus be written in terms of the Helmholtz and internal energies, while the isoparametric process at the high control parameter, associated with the heat Q_{AD} , is given by the difference in internal energies at fixed λ_H . At point D, the internal energy corresponds exclusively to the ground state due to the sufficiently low temperature. Thus, the expressions for the heats involved are given by

$$Q_{AB} = k_B T_H \ln \left(g_{\text{crit}} \right) - T_H S_{\lambda_H} (T_H), \qquad Q_{AD} = U_{\lambda_H} (T_H) - \epsilon_0. \tag{35}$$

Consequently, in the limit $\Delta \gg k_B T_L$, this term is negligible. Therefore, the heat exchanges for the complete cycle are:

$$Q_{AB} = T_H \left[S_{\lambda_{\text{crit}}}^{(B)}(T_H) - S_{\lambda_H}^{(A)}(T_H) \right] = k_B T_H \ln(g_{\text{crit}}) - U_{\lambda_H}^{(A)}(T_H) + F_{\lambda_H}^{(A)}(T_H), \tag{36}$$

$$Q_{BC} = U_{\lambda_{crit}}^{(C)}(T_L) - U_{\lambda_{crit}}^{(B)}(T_H) = 0, \tag{37}$$

$$Q_{CD} = T_L \left[S_{\lambda_H}^{(D)}(T_L) - S_{\lambda_{\text{crit}}}^{(C)}(T_L) \right] = k_B T_L \left[\ln(g_0) - \ln(g_{\text{crit}}) \right] = -k_B T_L \ln\left(\frac{g_{\text{crit}}}{g_0}\right), \tag{38}$$

$$Q_{DA} = U_{\lambda_H}^{(A)}(T_H) - U_{\lambda_H}^{(D)}(T_L) = U_{\lambda_H}^{(A)}(T_H) - \epsilon_0.$$
(39)

The work in the Stirling cycle is calculated as the sum of all heat exchanges. As seen, the internal energy terms cancel, yielding a contribution corresponding to the free energy component:

$$W = k_B T_L \ln \left(\frac{g_{\text{crit}}}{g_0} \right) + k_B T_H \ln \left(g_{\text{crit}} \right) + F_{\lambda_H}^{(A)} \left(T_H \right) - \epsilon_0. \tag{40}$$

By explicitly substituting the free energy from Eq.(33) into Eq.(40), the terms associated with the ground state cancel out, yielding

$$W = k_B \delta \ln \left(\frac{g_{\text{crit}}}{g_0} \right) - k_B (T_L + \delta) \ln \left(1 + \frac{g_1}{g_0} e^{-\frac{\Delta}{k_B (T_L + \delta)}} \right). \tag{41}$$

It is observed that, in the limit of a large energy gap, the previous result from Eq. (24) is recovered with an additional contribution at the Carnot limit. However, the thermal population of the first excited state reduces the useful work. To investigate its impact, the system efficiency is now analyzed from Eq. (13) substituting the heat terms from Eqs. (36–39). The resulting expression can be written as follows

$$\eta = 1 - \frac{k_B T_L \ln\left(\frac{g_{\text{crit}}}{g_0}\right)}{k_B T_H \ln\left(\frac{g_{\text{crit}}}{g_0}\right) - k_B T_H \ln\left(1 + \frac{g_1}{g_0}e^{-\frac{\Delta}{k_B T_H}}\right)}.$$
(42)

To account for the correction introduced by the heat term Q_{AD} to Carnot efficiency, Eq. (24) is expanded as a power series. Since the critical point involves the degeneracies g_0 and g_1 , the condition $\ln\left(1+\frac{g_1}{g_0}e^{-\Delta/(k_BT_H)}\right)<\ln\left(\frac{g_{\rm crit}}{g_0}\right)$ is always satisfied, enabling a geometric expansion. The result can then be expressed in terms of the Carnot efficiency as

$$\eta = \eta_C - \frac{T_L}{T_H} \sum_{n=1}^{\infty} \left(\frac{\ln\left(1 + \frac{g_1}{g_0} e^{-\frac{\Delta}{k_B T_H}}\right)}{\ln\left(\frac{g_{\text{crit}}}{g_0}\right)} \right)^n.$$
(43)

Inclusion of higher thermal populations reduces the maximum attainable efficiency, keeping it strictly below the Carnot limit. This reduction arises because part of the thermal energy is expended in populating excited states rather than contributing to useful work. In the limit of a large energy gap and/or sufficiently low temperature, these corrections vanish, and the Carnot efficiency is asymptotically recovered.

IV. GENERAL FRAMEWORK FOR QUANTUM STIRLING CYCLES: VALIDATION AND APPLICATION TO CRITICAL SYSTEMS WITH FIBONACCI-TYPE DEGENERACIES

Having established the theoretical framework for both ideal critical cycles and systems with a small energy gap, we now validate these models against quantum systems with QCPs reported in the literature. This includes quantum

critical systems, quantum heat engines that reach Carnot efficiency, and exactly solvable models. We examine a range of systems with diverse interactions to validate the derived formulas through postdictions of previously reported results. Furthermore, we provide new predictions for systems exhibiting nontrivial degeneracies, such as the critical point degeneracies in open and closed quantum Ising chains, which are characterized by Fibonacci and Lucas numbers.

A. Validation Across Reported Quantum Systems

1. Two spin-1/2 systems

Two-qubit systems have been widely studied in condensed matter and quantum information literature, often with different types of interactions. To provide a unified framework for these cases, we introduce a generalized XXZ Hamiltonian that collects the most relevant contributions, written in natural units of the exchange constant J:

$$\hat{\mathcal{H}}_{2\,spin-1/2} = J(\hat{S}_1^x \hat{S}_2^x + \hat{S}_1^y \hat{S}_2^y) + J_z \hat{S}_1^z \hat{S}_2^z + B_z \hat{S}_{\text{tot}}^z + K_y (\hat{S}_{\text{tot}}^y)^2 + D\left(\hat{\mathbf{S}}_1 \times \hat{\mathbf{S}}_2\right) \cdot \hat{\mathbf{z}}. \tag{44}$$

The Hamiltonian in Eq. (44) incorporates several fundamental interactions within the standard spin-operator formalism. The antiferromagnetic exchange constant J couples nearest-neighbor spins through a Heisenberg XX interaction, where the spin operators $\hat{S}_i = (\hat{S}_i^x, \hat{S}_i^y, \hat{S}_i^z)$ satisfy the usual angular momentum commutation relations. The total spin components are defined as $\hat{S}_{\text{tot}}^{\alpha} = \sum_{i=1}^{N} \hat{S}_i^{\alpha}$ with $\alpha \in \{x, y, z\}$. The J_z term couples the z-components of both spins, and for $J_z = J$ the system reduces to the isotropic Heisenberg XXX model. The Zeeman term, proportional to B_z , corresponds to a homogeneous magnetic field applied along the z axis. The uniaxial magnetic anisotropy K_y couples to the square of the total y-component of spin. Finally, the Dzyaloshinskii–Moriya interaction (DMI), parameterized by D, introduces an antisymmetric exchange that breaks inversion symmetry.

By selectively enabling or suppressing interaction terms, previously reported two-qubit models can be recovered as limiting cases of the general Hamiltonian. This construction provides a unified framework within which our formula can be benchmarked against diverse quantum configurations operating as Stirling engines. The corresponding parameter sets and the quantitative agreement are summarized in Table II.

Interaction	Mobile param.	λ_L	λ_H	T_L	T_H	$g_{ m crit}$	g_0	$W_{ m sim}$	$W_{ m formula}$	Error
$J = 1 \& D = 0$ $K_y = J_z = 0$ Purkait et al. [29]	B_z	1	3	0.15	0.25	2	1	0.0693147	$0.1 \ln 2$	4.0×10^{-7}
$J = 1, K_y = 0.5$ $J_z = D = 0$ Araya et al. [33]	B_z	$\sqrt{2}$	3	0.12	0.20	2	1	0.0693147	$0.08 \ln 2$	1.6×10^{-5}
$J = 1, K_y = 0$ $2D = J_z = 1$ Pili et al. [35]	B_z	1.06	4	0.10	0.20	2	1	0.0693161	$0.1 \ln 2$	2.0×10^{-5}
$B = D = 0$ $K_y = J_z = 0$ Cruz et al. [26]	J	-2.75	-1	20	25	4	1	6.90505	$5 \ln 4$	7.7×10^{-3}

TABLE II: Comparison of the generalized two-qubit Hamiltonian under different interaction configurations, operating as a quantum Stirling engine. The table lists the parameter sets considered, together with the corresponding degeneracies, simulated work output (W_{sim}) , and the predictions of the analytical expression (W_{formula}) . Temperatures and work are given in units of k_B , while the mobile parameter is expressed in exchange-constant units.

Table II summarizes several interaction configurations of the Hamiltonian in Eq.(44) along with their corresponding references. The mobile parameter varies between models, though the magnetic field is most commonly employed as the control variable. Thermal reservoirs are set at low and closely spaced temperatures. The simulated work output

 W_{sim} , given in units of k_B , is obtained from full numerical calculations and compared with the analytical prediction of Eq.(23), which depends solely on degeneracies and temperature differences for systems operating at Carnot efficiency.

In the case of the pure Heisenberg XX model, Purkait and Biswas [29] identified a QCP at B=1 with a twofold critical degeneracy. For B=3, where the ground state is non-degenerate, and temperatures $T_L=0.15$ and $T_H=0.25$, the system reaches Carnot efficiency, and the simulated work matches precisely the prediction of Eq. (23).

Introducing a planar anisotropy of $K_y = 0.5$, Araya et al. [33] showed that the critical field shifts to $B \simeq \sqrt{2}$ while preserving the twofold degeneracy. With B = 3 as the high-field parameter and temperatures $T_L = 0.12$ and $T_H = 0.20$, the work remains proportional to $\ln 2$, again in perfect agreement with the formula.

The combined effect of a homogeneous field and a Dzyaloshinskii–Moriya interaction was analyzed by Pili et al. [35]. For D=1/2, the critical point shifts to B=1.06, while the ground-state degeneracy remains unchanged. Operating the cycle with B=4, $T_L=0.10$, and $T_H=0.20$, the work continues to follow Eq. (23), demonstrating its robustness even away from the strict critical regime.

Cruz et al. [26] investigated an experimental dinuclear metal complex modeled as a two-qubit system with only nearest-neighbor interactions. Measurements of work, absorbed and released heat, and efficiency were found to be consistent with theoretical predictions. For the purposes of this manuscript, parameters around $J_L \simeq -2.75$ with reservoir temperatures $T_L = 20$ K and $T_H = 25$ K are considered. To further approach the critical regime at J = 0, the interaction is extended down to $J_H = -1$, slightly beyond the values reported in the experiment. In this range, the work output approaches the Carnot limit, though the deviation from Eq. (23) remains on the order of 10^{-3} due to the high-field point not coinciding exactly with the fourfold critical degeneracy. Extending the parameter closer to $J \simeq 0$ restores agreement with errors as small as 10^{-10} , although such conditions would not correspond to physically realizable parameters in an endoreversible cycle.

2. Nth spin-s system

The two–qubit benchmarks establish quantitative agreement between the analytical expression in Eq. (23) and simulated work across distinct interaction channels. The next step is to probe robustness beyond the minimal local Hilbert space and to assess the role of topology. This requires moving to higher on–site spin and to extended geometries (open chains vs. rings), for which a compact many–body description is provided below.

Recent studies demonstrate that topology, system size, and on-site spin magnitude significantly influence quantum thermal machine performance. To capture these effects systematically, we introduce a generalized Heisenberg-type Hamiltonian for chains of N spin-s sites:

$$\hat{\mathcal{H}}_{\text{spin-s}}^{(N)} = J \sum_{i=1}^{N-1} \hat{\mathbf{S}}_i \cdot \hat{\mathbf{S}}_{i+1} + B \hat{S}_{\text{tot}}^z + K_y \left(\hat{S}_{\text{tot}}^y \right)^2 + K_z \sum_{i=1}^N \left(\hat{S}_i^z \right)^2.$$
 (45)

This Hamiltonian (45) integrates the key interactions previously established: Heisenberg XXX exchange coupling (J), Zeeman field (B), easy-plane anisotropy (K_y) , and single-ion anisotropy (K_z) that promotes alignment of individual spins along the z-axis. When the summation is extended to N terms and periodic boundary conditions are imposed $(\hat{\mathbf{S}}_{N+1} \equiv \hat{\mathbf{S}}_1)$, the Hamiltonian can describe either open chains or closed rings, enabling systematic exploration of topological effects on work extraction and efficiency in quantum Stirling cycles.

This framework provides a unified foundation for analyzing how spin magnitude (s), geometry, and interaction symmetry shape the performance of quantum thermal devices. Table III compares representative cases of quantum Stirling engines with the analytical expression in Eq. (23) at Carnot efficiency. The results show consistent agreement between simulations and theory across different geometries, interaction types, and system sizes, with the magnetic field acting as the control parameter and thermal reservoirs maintained at low, closely spaced temperatures.

Castorene et al. [34] investigated isotropic Heisenberg XXX chains and rings of three qubits with a uniaxial anisotropy along the y-axis, using the magnetic field as the control parameter. As discussed earlier, such anisotropy shifts the critical field without altering the degeneracy structure. For a critical field at $B \simeq 2.41$ and a high-field point at B = 3.5, with reservoirs at $T_L = 0.15$ and $T_H = 0.25$, the work output followed Eq. (23) in both geometries. Notably, the ring configuration exhibited a larger work output, which can be attributed to the additional translational symmetry at zero field, yielding one extra critical degeneracy compared to the open chain.

In a different study, Castorene et al. [24] analyzed isotropic spin-1 dimers with single-ion anisotropy along the z-axis and an external magnetic field of opposite sign, which introduces frustration in the energy levels. Specific anisotropy values induce either a triple degeneracy point (TDP) at $K_z = -2/3$ or double degeneracy points (DDPs) at $K_z = -1/10$, each associated with critical magnetic fields. For instance, at B = 4/3 the system exhibits a TDP,

Interaction	Mobile param.	λ_L	λ_H	T_L	T_H	$g_{ m crit}$	g_0	$W_{ m sim}$	$W_{ m formula}$	Error
$J=1\ \&\ {f Chain}$										
$K_y = -0.44$										
$K_z = 0$	B	2.412	3.5	0.25	0.15	2	1	0.0692511	$0.1 \ln 2$	9.1×10^{-4}
Castorene et al. [34]										
(N = 3, Spin-1/2)										
$J=1\ \&\ \mathbf{Ring}$										
$K_y = -0.44$										
$K_z = 0$	B	2.412	3.5	0.25	0.15	3	1	0.109734	$0.1 \ln 3$	1.1×10^{-3}
Castorene et al. [34]										
(N = 3, Spin-1/2)										
$J=1\ \&\ {f Chain}$										
$\mathbf{K_z} = -2/3$										
$K_y = 0$	B	4/3	3.0	0.10	0.05	3	1	0.054973	$0.05 \ln 3$	7.7×10^{-4}
Castorene et al. [24]										
(N = 2, Spin-1)										
$J=1\ \&\ {f Chain}$										
$\mathbf{K_z} = -1/10$										
$K_y = 0$	B	1.90	3.0	0.10	0.05	2	1	0.0346646	$0.05 \ln 2$	2.0×10^{-4}
Castorene et al. [24]										
(N = 2, Spin-1)										

TABLE III: Comparison of the generalized spin-s chain Hamiltonian (45) for different interaction configurations and system sizes N, operating as quantum Stirling engines. The table reports the parameter sets, critical degeneracies, simulated work output (W_{sim}) , and the predictions of Eq. (23), showing quantitative agreement with results reported in the literature. Temperatures and work are given in units of k_B , while the mobile parameter is expressed in exchange-constant units.

while at $B \simeq 1.90$ one of the DDPs emerges. Stirling cycles performed with $B_H = 3.0$ and reservoirs at $T_L = 0.05$ and $T_H = 0.10$ yielded work outputs proportional to $\ln 3$ and $\ln 2$, respectively, in full agreement with Eq. (23).

Overall, these results highlight the robustness of the proposed framework across diverse quantum critical scenarios. The analytical expression for the work remains valid not only for two-qubit systems with additional interactions such as Dzyaloshinskii–Moriya coupling or planar anisotropy, but also for extended configurations involving higher spins, distinct topologies (chains and rings), and complex local anisotropies. This universality underscores the broad applicability of Eq. (23) to quantum thermal devices operating near criticality.

To further demonstrate the generality of the approach, an additional analysis of a non-Heisenberg spin model, the Lipkin–Meshkov–Glick (LMG) model, was carried out in Appendix A. The results confirm that the proposed formula remains accurate even for systems characterized by collective spin interactions and more intricate energy landscapes.

B. Quantum Ising model at criticality with Fibonacci-Lucas Degeneracies

The scalability of the work formula can be addressed by considering systems with an increasing number of interacting particles. A natural case study is the quantum antiferromagnetic Ising model in the z direction, one of the simplest many-body systems that exhibits a non-trivial QCP. The model is studied under a longitudinal magnetic field applied along the z axis, which drives the transition and enables exploration of how critical degeneracies scale with system size. The Hamiltonian of this system is given by

$$\hat{\mathcal{H}} = J \sum_{i=1}^{N-1} S_i^z S_{i+1}^z + B \sum_{i=1}^N S_i^z.$$
 (46)

This Hamiltonian describes a chain of N qubits with nearest–neighbor antiferromagnetic interactions. The exchange constant J denotes the isotropic antiferromagnetic coupling constant between adjacent spins (J>0), while \hat{S}^z_i represents the Pauli operator along the z direction. The longitudinal external magnetic field B is applied along the positive z axis and, in physical units, is given by $B=\mu_Bg_zH$, where μ_B is the Bohr magneton and g_z the Landé g-factor. For convenience, B is expressed in units of the exchange constant. Extending the summation to N terms with the identification $\hat{S}^z_{N+1}=\hat{S}^z_1$ imposes periodic boundary conditions, thereby mapping the open chain system onto a closed spin ring.

In this framework, the system exhibits a QCP at finite field, which occurs when the ratio B/J = 1. Such criticality arises for both open chains and closed rings of arbitrary length $N \ge 3$.

Correspondingly, the ground-state energy at the critical field and beyond, with respect to the magnetic field, is given by [40]

$$\epsilon_{\text{Ising}}^{(\text{ground})} = \frac{J}{4}(N-1) - \frac{NB}{2}, \qquad \frac{J}{B} \ge 1.$$
(47)

For periodic boundary conditions, the factor accompanying the exchange constant J extends as $(N-1) \to N$, while the magnetic field term remains unchanged. This implies that the open-chain geometry possesses a lower ground-state energy than the closed ring.

Accordingly, the Stirling cycle shown in Fig. 2 is implemented by driving the system from the quantum critical point at $\lambda_L = B/J = 1$ to a higher magnetic field $\lambda_H = B/J = 3$. The process is simulated within the canonical ensemble over the complete set of 2^N energy levels for both the open-chain and closed-ring geometries. This framework allows a direct comparison between the numerically computed work outputs $(W_{\text{Ising}}^{\text{Chain}}, W_{\text{Ising}}^{\text{Ring}})$ and the analytical prediction from Eq. (23), valid for arbitrary system size N. To establish this connection, it is necessary to determine how the critical ground-state degeneracy associated with the ground-state energy of Eq. (47) scales with N. In this context, recent studies [40, 41] showed that, for one-dimensional antiferromagnetic Ising model, the degeneracy at the QCP follows the Fibonacci sequence F_N , defined recursively as $F_N = F_{N-1} + F_{N-2}$ with $F_0 = F_1 = 1$. In contrast, periodic boundary conditions give rise to a nontrivial degeneracy governed by the Lucas sequence, which can be expressed in terms of the Fibonacci numbers as $L_N = F_{N+1} + F_{N-1}$. Using Binet's formula, both sequences can be written in closed form through the golden ratio $\varphi = (1 + \sqrt{5})/2$:

$$F_N = \frac{\varphi^N - (-\varphi^{-1})^N}{\sqrt{5}}, \qquad L_N = \varphi^N + (-1)^N \varphi^{-N}.$$
 (48)

Thus, performing the Stirling cycle from the QCP at B/J=1, where the Fibonacci–Lucas degeneracies of Eq. (48) apply, to a high-field configuration at B/J=3 with a non-degenerate ground state yields

$$W_{\text{Formula}}^{\text{Chain}} = k_B \delta \ln \left(\frac{\varphi^N - \left(-\varphi^{-1} \right)^N}{\sqrt{5}} \right), \tag{49}$$

$$W_{\text{Formula}}^{\text{Ring}} = k_B \delta \ln \left(\varphi^N - \left(-\varphi^{-1} \right)^N \right). \tag{50}$$

These previous expressions can be treated for the case of small system sizes N, observing that the work of both the chain and the ring does not scale linearly with N, reflecting a genuinely quantum effect that contrasts with the classical thermodynamic expectation of extensivity. Specifically, Eq. (49) shows that the work for the chain is proportional to the N-th Fibonacci number, while for Eq. (50) depict that the ring follows the N-th Lucas number, with the chain producing less work.

In the asymptotic limit $N \gg 1$, the inverse golden-ratio (φ^{-N}) terms can be neglected, yielding the approximate expressions

$$W_{\text{Formula}}^{\text{Chain}} \xrightarrow[N \gg 1]{} Nk_B \delta \ln (\varphi) - k_B \delta \ln \sqrt{5},$$
 (51)

$$W_{\text{Formula}}^{\text{Ring}} \xrightarrow[N \gg 1]{} Nk_B \delta \ln(\varphi).$$
 (52)

Eqs. (51-52) show that both cases scale linearly with N, but the chain includes a constant offset of $-\ln\sqrt{5}$, highlighting a residual distinction between quantum thermodynamics and its classical counterpart. However, in the thermodynamic limit $N \gg 1$, the constant term becomes negligible, and both chain and ring topologies recover

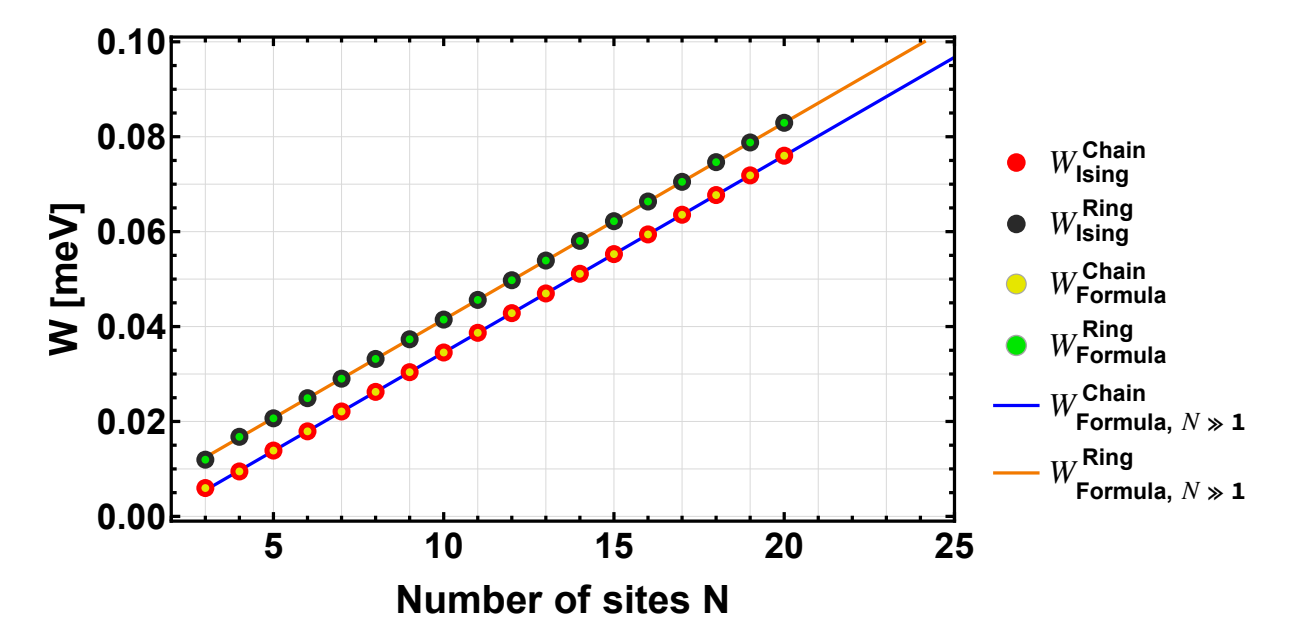


FIG. 4: Quantum Stirling work W [meV] as a function of the number of sites N for the antiferromagnetic Ising chain and ring (J=1), evaluated at the QCP $\lambda_L=B/J=1$ and a high-field parameter $\lambda_H=B/J=3$, with reservoir temperatures $T_L=0.1$ and $T_H=0.2$. In all cases the system operates at Carnot efficiency $\eta_C=0.5$. Red (black) dots represent simulated cycles for the chain (ring) system. Yellow and green markers show the predictions of Eqs. (49-50) based on Fibonacci and Lucas degeneracies at the QCP, respectively, while blue (orange) lines correspond to the large-N asymptotic expressions in Eqs. (51-52).

classical extensivity, yielding the same work output determined solely by the system size. This behavior is consistent with results reported in the literature for the classical Ising model.

Finally, Fig. 4 summarizes the main results, displaying the quantum Stirling work W as a function of the system size N for both open-chain and closed-ring configurations of the antiferromagnetic Ising model. The numerical simulations (red and black markers) exhibit excellent agreement with the analytical predictions derived from the Fibonacci and Lucas degeneracies (yellow and green markers), as well as with the large-N asymptotic limits (blue and orange lines). This consistency across sizes and topologies demonstrates the robustness and general validity of the proposed theoretical framework.

V. CONCLUSIONS

We have performed a comprehensive thermodynamic analysis of quantum systems exhibiting a QCP induced by a control parameter at zero temperature, using the canonical ensemble formalism. From these quantities, a quantum Stirling cycle was constructed under sufficiently low temperatures such that only the ground state remains significantly populated. The cycle begins at the QCP, characterized by critical degeneracy, and ends at a higher control parameter where the ground state becomes energetically isolated from the excited manifold.

This framework yields analytical expressions for the finite net work and Carnot-like efficiency in terms of the temperature difference between the thermal reservoirs and the ratio between the degeneracies of the critical and isolated ground state. The role of finite-temperature effects was also examined, revealing that partial thermal occupation of excited states reduces both useful work and maximum efficiency due to energy redistribution within the system.

The proposed work expression was validated through postdictions and predictions across diverse spin-s Heisenberg systems, incorporating Dzyaloshinskii–Moriya interactions, uniform magnetic fields, uniaxial anisotropies, and single-ion anisotropies. These results confirm the robustness of the formulation for systems operating near the Carnot regime.

Finally, the extensivity of the work output was analyzed for one-dimensional antiferromagnetic Ising systems with open-chain and closed-ring topologies of length N. The work was found to scale with the logarithm of the Nth Fibonacci number for open chains and with the logarithm of the Nth Lucas number for rings, indicating a higher useful work in closed geometries for small N. In the thermodynamic limit, both configurations converge to a linear dependence on N, thereby recovering the classical extensivity of the work.

ACKNOWLEDGMENTS

Authors acknowledge partial support from ANID CIA 250002, Fondecyt Grant (Chile) under contracts 1230055, 1240582 and 1250173. B.C. acknowledges support from Pontificia Universidad Católica de Valparaíso (PUCV) and the Dirección de Postgrado of Universidad Técnica Federico Santa María (UTFSM). B.C. also acknowledges the support of ANID Becas/Doctorado Nacional 21250015.

AUTHOR CONTRIBUTIONS

Bastian Castorene • — Conceptualization (lead), Data curation (lead), Formal analysis (lead), Investigation (lead), Methodology (lead), Visualization (lead), Writing – original draft (lead), Writing – review & editing (lead).

Martin HvE Groves • — Formal analysis (equal), Investigation (supporting), Validation (equal), Writing – review & editing (lead).

Francisco J. Peña • — Investigation (supporting), Supervision (equal), Validation (lead), Writing – review & editing (lead).

Eugenio E. Vogel • — Conceptualization (supporting), Funding acquisition (lead), Supervision (equal), Validation (equal), Writing – review & editing (supporting).

Patricio Vargas • — Conceptualization (lead), Methodology (lead), Supervision (lead), Writing – original draft (supporting), Writing – review & editing (equal).

DATA AVAILABILITY STATEMENT

Data sharing is not applicable to this article as no new data were created or analyzed in this study.

Appendix A: Applications in the Lipkin-Meshkov-Glick model

The Lipkin–Meshkov–Glick (LMG) model constitutes a paradigmatic framework in quantum many-body physics, extensively investigated in various experimental platforms such as Bose–Einstein condensates and trapped-ion systems [25]. Recent studies have shown that a quantum Stirling cycle employing the LMG model as its working substance can, under appropriate conditions, reach Carnot efficiency.

The model describes a system of N collectively interacting spins subjected to a uniform magnetic field, incorporating both symmetric and anisotropic spin–spin couplings. Its general Hamiltonian can be written as

$$\hat{\mathcal{H}}_{LMG} = \varepsilon S_z + V \left(S_x^2 - S_y^2 \right) + W \left(S^2 - S_z^2 \right), \tag{A1}$$

where $S_{\alpha} = \frac{1}{2} \sum_{i=1}^{N} \sigma_{i}^{\alpha}$ denotes the collective spin operators, and σ_{i}^{α} are the Pauli matrices acting on the *i*-th spin. The first term represents the Zeeman interaction with an external magnetic field of strength ε , while $S^{2} = S_{x}^{2} + S_{y}^{2} + S_{z}^{2}$ corresponds to the total spin magnitude. The coefficients V and W quantify the anisotropic components of the collective spin–spin coupling.

It is convenient to define the following dimensionless control parameters:

$$\lambda = -\frac{\varepsilon}{2}, \qquad \frac{\lambda_0}{N} = -\frac{W+V}{2}, \qquad \gamma = \frac{W-V}{W+V}.$$
 (A2)

In the isotropic case $\gamma = 1$, the Hamiltonian simplifies to

$$\hat{\mathcal{H}}_{LMG} = -\frac{2\lambda_0}{N} \left(S^2 - S_z^2 \right) - 2\lambda S_z. \tag{A3}$$

By setting $\lambda_0 = 1$, the energy eigenvalues take the compact form

$$E(M) = \frac{2}{N} \left(M - \frac{N\lambda}{2} \right)^2 - \frac{N}{2} \left(1 + \lambda^2 \right) - 1, \tag{A4}$$

where M assumes discrete values $M \in [-N/2, N/2]$.

This collective-spin model fulfills the general requirements for a quantum working substance discussed in the main text. Accordingly, the thermodynamic formalism developed earlier can be directly applied. For N=3 and N=4 the corresponding quantum Stirling cycles are constructed from the energy spectrum given in Eq. (A4), where the parameter λ acts as the external thermodynamic variable controlling the energy-level structure throughout the cycle.

Mobile param.	λ_L	λ_H	T_L	T_H	$g_{ m crit}$	g_0	$W_{ m sim}$	$W_{ m formula}$	Error
$\lambda $ (N = 3)	0.66	2.5	0.10	0.20	2	1	0.0694418	$0.1 \ln 2$	1.83×10^{-3}
$\lambda $ $(N = 4)$	0.75	4.0	0.15	0.30	2	1	0.0940877	$0.15 \ln 2$	4.77×10^{-2}

TABLE IV: Performance of the Lipkin–Meshkov–Glick (LMG) model operating as a quantum Stirling engine for different parameter sets and system sizes N=3 and N=4, respectively. The table lists the control parameters λ_L and λ_H , the reservoir temperatures T_L and T_H , the critical degeneracy $g_{\rm crit}$, the ground-state degeneracy g_0 , and the corresponding work output obtained from simulations ($W_{\rm sim}$) compared with the analytical prediction of Eq. (23). Quantities are expressed in units of k_B for temperature and work, while λ is given in dimensionless form. Results show quantitative agreement with Ref. [25].

The excellent agreement between the simulated and analytical results, evidenced by the negligible relative error, confirms the consistency and reliability of our approach. Moreover, for the parameter sets presented in Table IV, the quantum Stirling engine based on the Lipkin–Meshkov–Glick model operates at the Carnot efficiency limit, demonstrating the thermodynamic optimality of the system under the specified conditions. This result further highlights the versatility of the proposed formulation, which remains valid beyond Heisenberg-type spin models and successfully extends to collectively interacting systems such as the LMG model.

ACKNOWLEDGMENTS

Authors acknowledge partial support from ANID CIA 250002, Fondecyt Grant (Chile) under contracts 1230055, 1240582 and 1250173. B.C. acknowledges support from Pontificia Universidad Católica de Valparaíso (PUCV) and the Dirección de Postgrado of Universidad Técnica Federico Santa María (UTFSM). B.C. also acknowledges the support of ANID Becas/Doctorado Nacional 21250015.

S. Vinjanampathy and J. Anders, Quantum thermodynamics, Contemporary Physics 57, 10.1080/00107514.2016.1201896 (2016).

^[2] R. Kosloff and L. Amikam, Quantum heat engines and refrigerators: Continuous devices, Annual Review of Physical Chemistry 64, 365 (2014).

^[3] M. J. Henrich, F. Rempp, and G. Mahler, Quantum thermodynamic otto machines: A spin-system approach, EUROPEAN PHYSICAL JOURNAL-SPECIAL TOPICS 151, 157 (2007).

 ^[4] G. Katz and R. Kosloff, Quantum thermodynamics in strong coupling: Heat transport and refrigeration, ENTROPY 18, 10.3390/e18050186 (2016).

^[5] P. Skrzypczyk, A. J. Short, and S. Popescu, Work extraction and thermodynamics for individual quantum systems, Nature Communications 5, 4185 (2014).

^[6] X. He and J. He, Thermal entangled four-level quantum otto heat engine, Science China Physics, Mechanics and Astronomy 55, 1751 (2012).

^[7] A. E. Allahverdyan and T. M. Nieuwenhuizen, Extraction of work from a single thermal bath in the quantum regime, Phys. Rev. Lett. 85, 1799 (2000).

^[8] M. F. Frenzel, D. Jennings, and T. Rudolph, Reexamination of pure qubit work extraction., Physical review. E, Statistical, nonlinear, and soft matter physics **90** 5-1, 052136 (2014).

^[9] S. Ahadpour and F. Mirmasoudi, Coupled two-qubit engine and refrigerator in heisenberg model, Quantum Information Processing 20, 63 (2021).

- [10] S. Deffner, Efficiency of harmonic quantum otto engines at maximal power, ENTROPY 20, 10.3390/e20110875 (2018).
- [11] F. J. Peña, O. Negrete, N. Cortés, and P. Vargas, Otto engine: Classical and quantum approach, Entropy 22, 10.3390/e22070755 (2020).
- [12] F. J. Pena, D. Zambrano, O. Negrete, G. De Chiara, P. A. Orellana, and P. Vargas, Quasistatic and quantum-adiabatic otto engine for a two-dimensional material: The case of a graphene quantum dot, PHYSICAL REVIEW E 101, 10.1103/Phys-RevE.101.012116 (2020).
- [13] N. M. Myers, O. Abah, and S. Deffner, Quantum thermodynamic devices: From theoretical proposals to experimental reality, AVS quantum science 4 (2022).
- [14] C. Myatt, B. King, Q. Turchette, C. Sackett, D. Kielpinski, W. Itano, C. Monroe, and D. Wineland, Decoherence of quantum superpositions through coupling to engineered reservoirs, Nature 403, 269 (2000).
- [15] T. Kieu, The second law, maxwell's demon, and work derivable from quantum heat engines, Physical Review Letters 93, 140403 (2004).
- [16] E. Geva and R. Kosloff, On the classical limit of quantum thermodynamics in finite-time, JOURNAL OF CHEMICAL PHYSICS 97, 4398 (1992).
- [17] H. M. Soufy and C. Benjamin, Flat-band thermodynamics reveals enhanced performance across otto, carnot, and stirling cycles, Phys. Rev. A , (2025).
- [18] X.-M. X. Xiao-Li Huang, Xin-Ya Niu and X.-X. Yi, Quantum stirling heat engine and refrigerator with single and coupled spin systems, The European Physical Journal D 68, 10.1140/epjb/e2013-40536-0 (2014).
- [19] A. H. B. Pili, R. Khordad, H. R. R. Sedehi, and A. Avazpour, Study of performance of quantum stirling engine using 2d and 3d heisenberg model, International Journal of Theoretical Physics 62, 192 (2023).
- [20] J.-Z. He, X. He, and Z. Jie, Entangled quantum heat engine based on two-qubit heisenberg xy model, Chinese Physics B CHIN PHYS B 21 (2012).
- [21] S. H. Raja, S. Maniscalco, G. S. Paraoanu, J. P. Pekola, and N. L. Gullo, Finite-time quantum stirling heat engine, New Journal of Physics 23 (2020).
- [22] T. Feldmann and R. Kosloff, Performance of discrete heat engines and heat pumps in finite time, Physical Review E 61, 10.1103/PhysRevE.61.4774 (2000).
- [23] R. J. de Assis, J. S. Sales, J. A. R. da Cunha, and N. G. de Almeida, Universal two-level quantum otto machine under a squeezed reservoir, Physical Review E 102, 052131 (2020).
- [24] B. Castorene, V. G. de Paula, F. J. Peña, C. Cruz, M. Reis, and P. Vargas, Quantum level-crossing induced by anisotropy in spin-1 heisenberg dimers: Applications to quantum stirling engines, Advanced Quantum Technologies 8, e2500204 (2025), https://advanced.onlinelibrary.wiley.com/doi/pdf/10.1002/qute.202500204.
- [25] Y.-H. Ma, S.-H. Su, and C.-P. Sun, Quantum thermodynamic cycle with quantum phase transition, Phys. Rev. E 96, 022143 (2017).
- [26] C. Cruz, H.-R. Rastegar-Sedehi, M. F. Anka, T. R. de Oliveira, and M. Reis, Quantum stirling engine based on dinuclear metal complexes, Quantum Science and Technology 8, 035010 (2023).
- [27] J. P. S. Peterson, T. B. Batalhao, M. Herrera, A. M. Souza, R. S. Sarthour, I. S. Oliveira, and R. M. Serra, Experimental characterization of a spin quantum heat engine, PHYSICAL REVIEW LETTERS 123, 10.1103/PhysRevLett.123.240601 (2019).
- [28] S. Sachdev, Quantum phase transitions (Cambridge university press, 2011).
- [29] C. Purkait and A. Biswas, Performance of heisenberg-coupled spins as quantum stirling heat machine near quantum critical point, Physics Letters A 442, 128180 (2022).
- [30] J.-Z. He, X. He, and J. Zheng, Thermal entangled quantum heat engine working with a three-qubit heisenberg xx model, INT. J. THEOR. PHYS. **51**, 2066 (2012).
- [31] X. Wang, H. Fu, and A. I. Solomon, Thermal entanglement in three-qubit heisenberg models, Journal of Physics A: Mathematical and General **34**, 11307 (2001).
- [32] T. Kiran and M. Ponmurugan, The invariant-based shortcut to adiabaticity for qubit heat engine operates under quantum otto cycle, The European Physical Journal Plus 137 (2022).
- [33] C. Araya, F. J. Pena, A. Norambuena, B. Castorene, and P. Vargas, Magnetic stirling cycle for qubits with anisotropy near the quantum critical point, TECHNOLOGIES 11, 10.3390/technologies11060169 (2023).
- [34] B. Castorene, F. J. Peña, A. Norambuena, S. E. Ulloa, C. Araya, and P. Vargas, Effects of magnetic anisotropy on three-qubit antiferromagnetic thermal machines, Phys. Rev. E 110, 044135 (2024).
- [35] A. H. B. Pili, R. Khordad, and H. R. R. Sedehi, Quantum stirling heat engine in two-coupled-qubit heisenberg xyz model, The European Physical Journal Plus 138, 871 (2023).
- [36] E. I. Kuznetsova, M. A. Yurischev, and S. Haddadi, Quantum otto heat engines on xyz spin working medium with dm and ksea interactions: operating modes and efficiency at maximal work output, QUANTUM INFORMATION PROCESSING 22, 192 (2023).
- [37] Y. Yin, L. Chen, and F. Wu, Performance of quantum stirling heat engine with numerous copies of extreme relativistic particles confined in 1d potential well, PHYSICA A-STATISTICAL MECHANICS AND ITS APPLICATIONS 503, 58 (2018).
- [38] K. Ono, S. N. Shevchenko, T. Mori, S. Moriyama, and F. Nori, Analog of a quantum heat engine using a single-spin qubit, Phys. Rev. Lett. 125, 166802 (2020).
- [39] C. M. S. da Conceicao and R. N. P. Maia, Recurrence relations in one-dimensional ising models, Phys. Rev. E **96**, 032121 (2017).
- [40] J. Zhang, F. M. Cucchietti, C. M. Chandrashekar, M. Laforest, C. A. Ryan, M. Ditty, A. Hubbard, J. K. Gamble, and

- R. Laflamme, Direct observation of quantum criticality in ising spin chains, Phys. Rev. A **79**, 012305 (2009). [41] D. V. Laptiev, O. O. Kryvchikov, Y. V. Savin, and V. V. Slavin, Magnetic properties of the frustrated ising chain, Low Temperature Physics **50**, 158 (2024).